

Supplementary Information

Highly efficient broadband multi-functional Metaplate

Azhar Javed Satti^{‡,a}, Muhammad Ashar Naveed^{‡,b}, Isma Javed^a, Nasir Mahmood^c, Muhammad Zubair^a, Muhammad Qasim Mehmood^{*,a}, Yehia Massoud^{*,c}

Azhar Javed Satti^a, Isma Javed^a, Muhammad Zubair, Prof. Muhammad Qasim Mehmood

^aMicroNano Lab, Department of Electrical Engineering, Information Technology University of the Punjab, Ferozpur Road, Lahore 54600, Pakistan

E-mail: qasim.mehmood@itu.edu.pk

Muhammad Ashar Naveed^b

^bDepartment of Electrical and Computer Engineering, University of Nebraska-Lincoln, Lincoln, NE 68588, United States.

Nasir Mahmood^c, Prof. Yehia Massoud^{*,c}

^cInnovative Technologies Laboratories (ITL), King Abdullah University of Science and Technology (KAUST), Thuwal 23955, Saudi Arabia

E-mail: *yehia.massoud@kaust.edu.sa

[‡] These authors contributed equally to this work.

Supplementary Section 1: Optimization graph Co-polarized transmission

The total transmission efficiency of the metaresonator is the combination of co- and cross-polarization efficiencies. These efficiencies depend on the nano-bar's physical parameters, which may alter to give multiple resonance modes. In order to obtain anisotropic condition, the suggested optimization function in the main primary document, under provided constraints on choice variables in the context of physical parameters. Here, Optimization graphs for Ψ_{cr} for all operating wavelengths ($\lambda_1 = 488 \text{ nm}$, $\lambda_2 = 532 \text{ nm}$, and $\lambda_3 = 633 \text{ nm}$) are presented in Fig. S1.

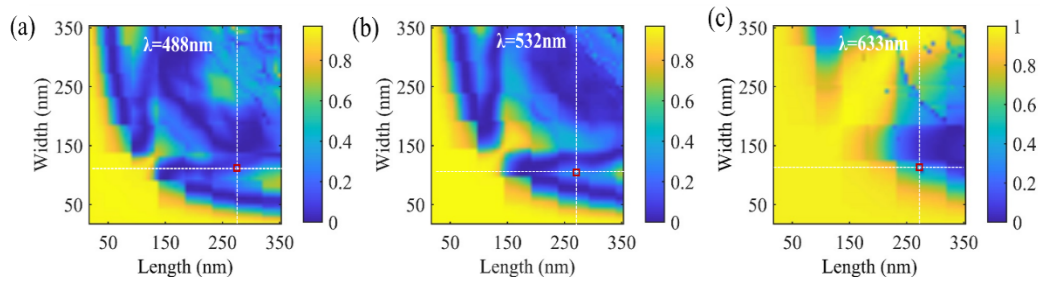


Fig. S1. Co-polarization effectiveness of the metaresonator is a function of its physical dimension length L and width W . To have autonomous control over orthogonal polarization, these physical dimensions are tuned to acquire the finest response, i.e., maximum cross-polarization efficiency points to have corresponding minimal co-polarization efficiency points. The objective function is augmented and plotted alongside three optical wavelengths (a) 488nm, (b) 532nm, and (c) 633nm of the visible regime in order to have a wideband response.

Supplementary Section 2: Magnetic resonances for the designed meta element

Fig. S2, illustrate the dielectric resonances for meta element at two working wavelengths ($\lambda_1 = 488 \text{ nm}$ and $\lambda_2 = 532 \text{ nm}$). Both electric and magnetic resonances occur and are well confined in the nano rectangular bar.

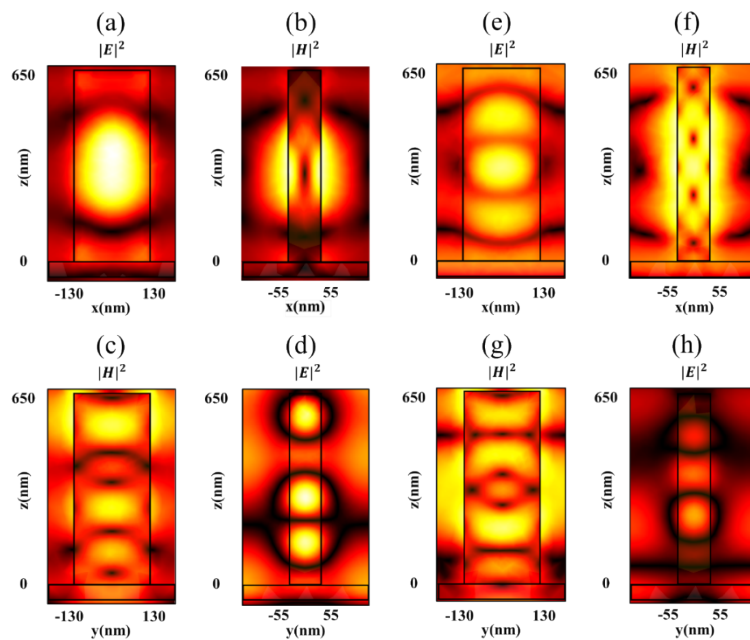


Fig. S2. Various resonance modes of ZnS-based anisotropic meta resonator. (a) The absolute electric field $|E|^2$ and (b) absolute magnetic field $|H|^2$ inside the bar under the influence of x-LP at an optical wavelength of 488nm. While (c) and (d) validates the $|H|^2$ and $|E|^2$ for y-LP light incidence for 488nm. Similarly, (e), (f) and (g), (h) depicts the fields inside the nano-rectangular bar for another optical wavelength of 532nm of both scenarios of the linear polarization. For both linear polarization scenarios, multiple resonances are provoked due to the intrinsic nature of dielectrics. This confines the electric field strongly inside the nano-bar and supports high transmission efficiency.

Supplementary Section 3: Mathematical estimation of hologram phase pattern

The mathematically calculated amplitude mask of the "DIAMOND" image and phase mask of the selected plane images of "BICYCLE" and "ROCKET" are represented in Fig. S3. A modified Gerchberg-Saxton (GS) algorithm is used to compute these phases for a $100 \times 100 \mu\text{m}^2$ metasurface.

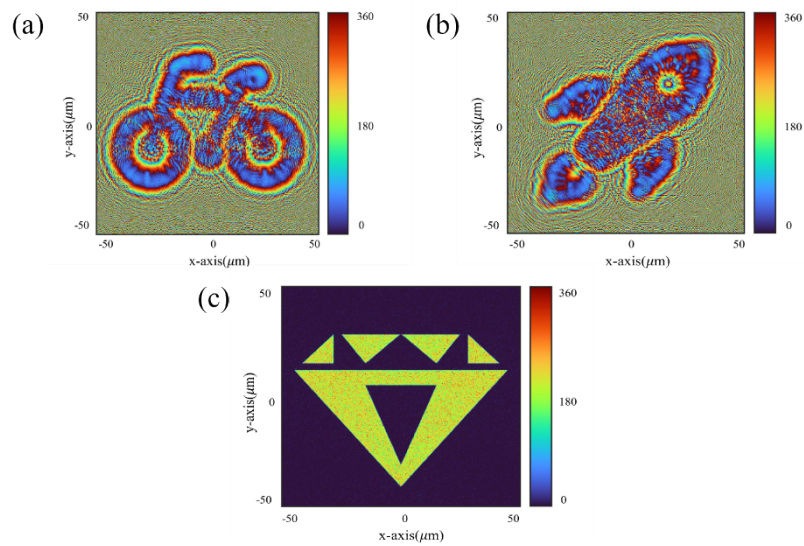


Fig. S3. Mathematically calculated phase and amplitude of different high-quality images for 243×243 array of meta-nanoresonators (a) Phase pattern of "BICYCLE" image calculated for LHCP, (b) Phase pattern of "ROCKET" image calculated for RHCP, (c) illustrates intensity modulation for "Diamond" picture.